Sublattice-Dependent Antiferromagnetic Transitions in Rare Earth Nickelates

Yin Shi* and Long-Qing Chen†
Department of Materials Science and Engineering, The Pennsylvania State University, University Park, Pennsylvania 16802, USA

(Received 30 November 2022; revised 5 March 2023; accepted 19 April 2023; published 3 May 2023)

Perovskite rare earth nickelates exhibit remarkably rich physics in their metal-insulator and antiferromagnetic transitions, and there has been a long-standing debate on whether their magnetic structures are collinear or noncollinear. Through symmetry consideration based on the Landau theory, we discover that the antiferromagnetic transitions on the two nonequivalent Ni sublattices occur separately at different Néel temperatures induced by the O breathing mode. It is manifested by two kinks on the temperature-dependent magnetic susceptibilities with the secondary kink being continuous in the collinear magnetic structure but discontinuous in the noncollinear one. The prediction on the secondary discontinuous kink is corroborated by an existing magnetic susceptibility measurement on bulk single-crystalline nickelates, thus strongly supporting the noncollinear nature of the magnetic structure in bulk nickelates, thereby shedding new light on the long-standing debate.

DOI: 10.1103/PhysRevLett.130.186801

Understanding spin and charge ordering and electronic correlation-induced metal-insulator (MI) transitions is one of the main research areas in condensed matter physics. These phenomena coexist in perovskite rare earth nickelates with the chemical formula $R\mathrm{NiO}_3$, where R denotes a rare earth element or a combination of rare earth elements. At high temperatures, the nickelates (except for $R = \mathrm{La}$) are metallic and paramagnetic and have an orthorhombic lattice structure with the space group $Pbnm$, while their ground states at low temperatures are insulating and antiferromagnetic (AFM) and have a monoclinic structure with the space group $P2_1/n$ [1]. The MI transition temperature T_{MI} and the Néel temperature T_N are correlated with the radii of the rare earth ions; T_{MI} decreases as the R^{3+}'s radius increases, and $T_{\mathrm{MI}} > T_N$ if R^{3+}'s radius is smaller than Nd^{3+}'s, and $T_{\mathrm{MI}} = T_N$ for larger ions $R = \mathrm{Nd}$, Pr [1,2]. The nickelate with the largest rare earth ion $R = \mathrm{La}$ is a rhombohedral metal down to near zero temperature but was recently found to have a finite Néel temperature $T_N = 157$ K [3].

The MI transition of the nickelates is always accompanied by the lattice distortion from $Pbnm$ to $P2_1/n$, resulting in two nonequivalent Ni sublattices. The O octahedra around Ni ions in one Ni sublattice denoted by Ni1 become larger than those in the other Ni sublattice denoted by Ni2, across the metal-to-insulator transition. This O breathing mode (bond disproportionation) was believed to be associated with a charge ordering on the Ni ions with nominal valences $\mathrm{Ni1}^{2+}$ and $\mathrm{Ni2}^{4+}$ inducing the MI transition [4–6], until most recent simulations supported a charge ordering in the form of ligand holes and a site-selective Mott transition induced by the O breathing mode [7–10].

Regardless of the mechanism of the MI transition, in the insulating AFM phase, Ni1 and Ni2 have nominal spins $S = 1$ and $S = 0$, respectively, and the actual magnetic moment on Ni1 is larger than that on Ni2, which is nonzero [4]. The magnetic moments within each Ni sublattice are antiparallel, while the moments between the two Ni sublattices in bulk could be either collinear or noncollinear, both compatible with the neutron powder diffraction data [4,11,12], so there has been a long-standing debate on whether the magnetic structure is collinear or noncollinear. The resulting spin density wave has a wave vector of $\boldsymbol{Q} = \pi(1, 0, 1)$ with respect to the $Pbnm$ lattice. X-ray resonant diffraction indicated that some members of the rare earth nickelates in the thin film or powder forms have the noncollinear magnetic structure [13–15].

Despite these extensive studies, none of them considered the possibility of different AFM transition characteristics on the two Ni sublattices. Here, we use symmetry analysis based on the Landau theory to provide insights into the sublattice-resolved AFM transitions. We find that the AFM transitions on the two Ni sublattices actually occur separately at different Néel temperatures, which is induced by the O breathing distortion through the lattice-spin interaction. We will call the AFM transition on the Ni1 (Ni2) sublattice the first (second) AFM transition hereafter. These separated AFM transitions each result in a kink on the temperature-dependent magnetic susceptibility, which is unambiguously corroborated by an existing susceptibility measurement. We show that the secondary kink can be used to distinguish the magnetic structure, and the analysis clearly supports the noncollinear nature of the magnetic structure, thus shedding new light on the long-standing debate.

The Landau theory of the rare earth nickelates has been established with the cubic phase as its reference; i.e., the order parameters carry irreducible representations of the cubic space group of ideal perovskites [16]. There have also been several existing theoretical analyses utilizing the Landau theory but primarily focusing on the nature of the MI transitions [17–19]. Here we consider the realistic orthorhombic symmetry of the disordered phase of the nickelates. The advantages of the phenomenological Landau theory are the insensitivity to the microscopic mechanism and the ease of properly accounting for the symmetry breaking of phase transitions. We determine that the order parameter characterizing the $Pbnm \to P2_1/n$ lattice distortion (previously interpreted as characterizing a charge density wave) η carries the real one-dimensional small representation Γ_3^+ of the $\boldsymbol{q} = (0,0,0)$ group of $Pbnm$ [20,21]. $\boldsymbol{q}$ is a reciprocal vector. η describes the relative change in the O octahedra size of the O breathing mode $\ell_j = \overline{\ell}[1 + \eta e^{i2\pi(x_j+z_j)}]$, where $\boldsymbol{r}_j = (x_j, y_j, z_j)$ are the fractional coordinates with respect to the orthorhombic unit cell of the jth Ni site. The order parameters characterizing the AFM order carry the real two-dimensional small representation T_2 of the $\boldsymbol{q} = \boldsymbol{Q}$ extended group of $Pbnm$ [20,21]. There are thus two real order parameters for the spin ordering $\boldsymbol{S}_1$ and $\boldsymbol{S}_2$, which can be the spins on the N11 and Ni2 sublattices, respectively. $\boldsymbol{S}_1$ and $\boldsymbol{S}_2$ are themselves three-dimensional spin vectors, which transform in the spin SU(2) space and thus play no role in the space group transformations [16]. The irreducible representations are listed in Table I.

$\boldsymbol{S}_1$ and $\boldsymbol{S}_2$ can be combined to form a complex vector $\boldsymbol{\psi} = \boldsymbol{S}_1 - i\boldsymbol{S}_2$, which is actually the $\boldsymbol{q} = \boldsymbol{Q}$ Fourier coefficient of the spin density wave, $\boldsymbol{S}_j = \Re[\boldsymbol{\psi} e^{i\boldsymbol{Q}\cdot\boldsymbol{r}_j}]$. $\Re[\cdot]$ means the real part. The resulting invariant Landau expansion up to the fourth order of the order parameters is

$$F(\eta,\boldsymbol{\psi}) = a_0\eta^2 + a_1\eta^4 + b_0\boldsymbol{\psi}^*\cdot\boldsymbol{\psi} + b_1(\boldsymbol{\psi}^*\cdot\boldsymbol{\psi})^2 + b_1'|\boldsymbol{\psi}\cdot\boldsymbol{\psi}|^2 + b_1''\Re[(\boldsymbol{\psi}\cdot\boldsymbol{\psi})^2] - k\eta\Re[\boldsymbol{\psi}\cdot\boldsymbol{\psi}]. \quad (1)$$

Note that unlike in the prior Landau theory [16], the $\Re[\boldsymbol{\psi}\cdot\boldsymbol{\psi}]$ term is not invariant under all the symmetry operations in $Pbnm$ and thus not allowed, which one can check using Table I. The constant k must be positive to respect the fact that Ni in the larger (smaller) O octahedron has the spin with the larger (smaller) magnitude S_1 (S_2).

TABLE I. Irreducible representations carried by the order parameters. The first row lists the rotational symmetry operations of $Pbnm$, where the subscripts a, b, and c represent the orthorhombic a, b, and c axes, respectively. The real two-dimensional irreducible representations are expressed in terms of the Pauli matrices σ_x, σ_y, and σ_z. I is the identity matrix.

	1	b	n	m	$\bar{1}$	2_{1a}	2_{1b}	2_{1c}
η	1	-1	1	-1	1	-1	1	-1
$(\boldsymbol{S}_1,\boldsymbol{S}_2)$	I	$-\sigma_x$	$-I$	σ_x	$-\sigma_z$	$-i\sigma_y$	σ_z	$i\sigma_y$

We consider a general solution $\boldsymbol{\psi} = |\psi|[e^{-i\theta}\cos(\phi/2)\hat{\boldsymbol{e}}_1 + e^{i\theta}\sin(\phi/2)\hat{\boldsymbol{e}}_2]$ yielding

$$\boldsymbol{S}_1 = |\psi|\cos(\theta)[\cos(\phi/2)\hat{\boldsymbol{e}}_1 + \sin(\phi/2)\hat{\boldsymbol{e}}_2], \quad (2)$$

$$\boldsymbol{S}_2 = |\psi|\sin(\theta)[\cos(\phi/2)\hat{\boldsymbol{e}}_1 - \sin(\phi/2)\hat{\boldsymbol{e}}_2], \quad (3)$$

where $\hat{\boldsymbol{e}}_1$ and $\hat{\boldsymbol{e}}_2$ are two perpendicular directions. This describes a general magnetic structure in which the magnitude ratio S_2/S_1 is $|\tan\theta|$ and the angle between $\boldsymbol{S}_1$ and $\boldsymbol{S}_2$ is ϕ. Plugging this solution into Eq. (1), we obtain the angle-dependent part of the expansion,

$$F_{\theta\phi} = (b_1' - b_1'')|\psi|^4\sin^2(2\theta)\cos^2\phi + (b_1' + b_1'')|\psi|^4\cos^2(2\theta) - k\eta|\psi|^2\cos(2\theta). \quad (4)$$

Let us consider $T \lesssim T_N$, so that $|\psi| \neq 0$. Minimization of Eq. (4) with respect to θ gives

$$\left\{\cos(2\theta) - \frac{k\eta}{2|\psi|^2[b_1'\sin^2\phi + b_1''(1+\cos^2\phi)]}\right\} \times \sin(2\theta) = 0, \quad (5)$$

which determines the equilibrium θ.

For the noncoincident MI and AFM transitions, the AFM transitions are second order [22–24], so η is finite and $|\psi| \to 0$ as $T \to T_N - 0$. Then it is obvious that Eq. (5) forces $\sin(2\theta) = 0$; i.e., $\theta = n\pi/2$, with n being an even (odd) integer for positive (negative) η determined by the equilibrium requirement $\partial^2 F_{\theta\phi}/\partial\theta^2 > 0$. This is true until $|\psi|$ ramps up from zero to a finite value $|\psi_{N2}|$ satisfying

$$|\psi_{N2}|^2 = \frac{k|\eta|}{2[b_1'\sin^2\phi + b_1''(1+\cos^2\phi)]}, \quad (6)$$

so that the expression inside the curly brackets in Eq. (5) can be zero. For this $\theta = n\pi/2$, the smaller spin is exactly zero, and Eq. (4) is independent of ϕ, meaning that the second AFM transition lags behind the first one by a finite temperature range as the temperature decreases. This is the case irrespective of whether the magnetic structure is collinear or not. Let us denote the Néel temperature of the second AFM transition by T_{N2}. An important conclusion drawn from Eq. (6) is that the separation of the AFM transitions on the two Ni sublattices is induced by the O breathing distortion.

For $T < T_{N2}$, i.e., $|\psi| > |\psi_{N2}|$, Eq. (5) gives the equilibrium θ a general value determined by

$$\cos(2\theta) = \mathrm{sgn}(\eta)\left|\frac{\psi_{N2}}{\psi}\right|^2, \quad (7)$$

which is more favored over $\theta = n\pi/2$ because of the equilibrium requirement $\partial^2 F_{\theta\phi}/\partial\phi^2 > 0$. From Eqs. (2) and (3), this means that S_1 and S_2 are unequal and both nonzero at low temperatures as found experimentally [4,12]. The equilibrium ϕ is given by the minimization of Eq. (4) with respect to ϕ, $\sin(2\phi) = 0$; i.e., $\phi = m\pi/2$ with m being an integer. m is even for $b_1' < b_1''$ and $b_1'' > 0$ or odd for $b_1' > |b_1''|$ determined by the equilibrium requirement $\partial^2 F_{\theta\phi}/\partial\theta^2 > 0$ and $\partial^2 F_{\theta\phi}/\partial\phi^2 > 0$ [$\partial^2 F_{\theta\phi}/(\partial\theta\partial\phi) = 0$ here]. From Eqs. (2) and (3), an even m corresponds to the collinear structure, while an odd m corresponds to the noncollinear structure in which $\boldsymbol{S}_1$ is perpendicular to $\boldsymbol{S}_2$. Therefore, the only symmetry-allowed noncollinear structure is that of perpendicular magnetic moments on the Ni1 and Ni2 sublattices.

Although occurring at different Néel temperatures, the first and second AFM transitions have the same critical exponent. Without loss of generality, let us consider $\eta > 0$. First, for $\delta T = T - T_N \to -0$ and using Eq. (2), one has $\theta = 0$ and the larger spin $S_1 = |\psi|\cos\theta = |\psi| \sim (-\delta T)^{1/2}$. Second, for $\delta T = T - T_{N2} \to -0$, i.e., $\delta|\psi| = |\psi| - |\psi_{N2}| \to +0$, we have $\sin^2\theta = [1 - \cos(2\theta)]/2 = \delta|\psi|/|\psi_{N2}| + o((\delta|\psi|)^2)$ using Eq. (7). Then, using Eq. (3), we have for the smaller spin

$$S_2^2 = |\psi|^2\sin^2\theta = |\psi_{N2}|\delta|\psi| + o((\delta|\psi|)^2)$$
$$= |\psi_{N2}|\delta S_1 + \frac{S_2^2}{2} + o((\delta S_1)^2) + o(S_2^3) + o(S_2^2\delta S_1),$$

where the second line is an expansion of $\delta|\psi|$ with respect to $\delta S_1 = S_1 - |\psi_{N2}|$ and $\delta S_2 = S_2$ around the second AFM transition point. Solving for S_2, one has

$$S_2 \sim (\delta S_1)^{1/2} = \left(\frac{dS_1}{dT}\bigg|_{T=T_{N2}-0}\delta T\right)^{1/2} \sim (-\delta T)^{1/2},$$

because $(dS_1/dT)|_{T=T_{N2}-0}$ is finite (which can be seen in Fig. 2). Therefore, the (mean-field) critical exponents of the two AFM transitions are both $\beta = 1/2$.

Compared to the noncoincident MI and AFM transitions, the coincident transitions have one difference: They are first order [24,25], meaning both η and $|\psi|$ are finite as $T \to T_N - 0$. Therefore, it becomes possible that Eq. (7) at $T = T_N - 0$ already has solutions for θ, rendering concurrent AFM transitions on the Ni1 and Ni2 sublattices. Whether this is the case depends on the particular values of the Landau parameters in Eq. (1). Either way, it is obvious that the lagging $T_N - T_{N2}$ for the coincident MI and AFM transitions should be smaller than that for the noncoincident transitions.

Now we show that the Landau theory is able to yield the correct phase diagram for various rare earth elements. First, it is normally assumed that the phase instability comes from the coefficients of the terms of the second order of the order parameters, a_0 and b_0. We use the simplest linear dependence of a_0 and b_0 on the temperature T and the tolerance factor τ, which depends on the radius of the rare earth ions and describes how much the lattice is distorted from the cubic symmetry. $a_0 = -a_0' + a_0''\tau + a_0'''T/T_0$ and $b_0 = -b_0' + b_0''\tau + b_0'''T/T_0$, where $T_0 = 298$ K is the room temperature. We fit all the parameters in Eq. (1) except the coefficients in front of T, a_0''', and b_0''' to the ground state energy as a function of τ (we use the experimental τ's [1] instead of the calculated ones) calculated by the density functional theory [26]. a_0''' and b_0''' are instead fitted to the experimentally measured $T_{\rm MI}$ and T_N for $R =$ Y, Nd [1]. The fitted parameters are listed in Table II. Numerically speaking, the collinear and noncollinear magnetic structures have the same form of the Landau free-energy expansion, which is indicated by their corresponding renormalizations of some of the Landau parameters in Table II. Therefore, they can exhibit the same phase diagram and magnitudes of the order parameters.

We can then calculate the τ-T phase diagram and compare it to the experimentally measured one in Fig. 1.

TABLE II. Landau parameters in units of meV f.u.$^{-1}$. $(\boldsymbol{\psi}^*\cdot\boldsymbol{\psi})^2 = |\boldsymbol{\psi}\cdot\boldsymbol{\psi}|^2$ ($|\boldsymbol{\psi}\cdot\boldsymbol{\psi}|^2 = \Re[(\boldsymbol{\psi}\cdot\boldsymbol{\psi})^2]$) for the collinear (noncollinear) structure, which is the reason for the renormalizations listed in the footnotes.

a_0'	a_0''	a_0'''	a_1	b_0'
353.15	376.11	14.41	119.10	−33.56
b_0''	b_0'''	$\tilde{b}_1'$ [a]	$\tilde{b}_1''$ [b]	k
−100.00	96.77	58.68	69.60	88.00

[a] $\tilde{b}_1' = b_1 + b_1' - b_1''$ ($\tilde{b}_1' = b_1$) for the collinear (noncollinear) structure.

[b] $\tilde{b}_1'' = 2b_1''$ ($\tilde{b}_1'' = b_1' + b_1''$) for the collinear (noncollinear) structure.

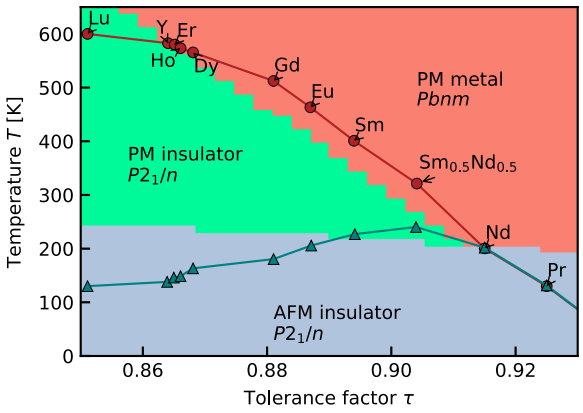

FIG. 1. Tolerance factor-temperature phase diagram. Color shades, calculated; markers, experimental [1]. The circles and triangles are the phase boundaries of the MI transition and AFM transition, respectively. The stairlike boundaries between the color shades are due to the finite number of data points.

The calculated phase boundaries are in fair agreement with the measured ones, especially reproducing both the coincident and noncoincident MI and AFM transitions. Figure 2 shows the calculated order parameters as functions of the temperature for $R = Y$, Pr. The noncoincident MI and AFM transitions for $R =$ Y are both second order, which is an outcome of the Landau expansion used, while a weak first-order nature was observed in experiments [4,23,27]. The first-order nature can be reproduced by the Landau theory with explicit incorporation of the electronic degrees of freedom [18,19]. The coincident MI and AFM transitions for $R =$ Pr are first order [1,16,26]. The first and the second AFM transitions clearly occur at different Néel temperatures for both $R = Y$, Pr, and the Néel temperature difference for $R =$ Y is larger than that for $R =$ Pr, as proven in the above theory.

We finally present the magnetic susceptibilities of $LuNiO_3$ and $YNiO_3$ calculated for both the collinear and noncollinear structures and compare them to an existing susceptibility measurement for the corresponding single crystals [27]. We choose these two nickelates because among the commonly used rare earth elements in nickelates, Lu and Y are the only two that are nonmagnetic, which is thus convenient for one to investigate only the magnetic properties of the Ni sublattice. We briefly explain how to calculate the magnetic susceptibility here. The magnetic moments within the Ni1 or Ni2 sublattice are AFM, so upon applying an external magnetic field $\boldsymbol{H}$, one needs to distinguish the spin-up and spin-down sublattices within the Ni1 or Ni2 sublattice. Let us denote $\boldsymbol{\psi}$ on the spin-up and spin-down sublattices by $\boldsymbol{\psi}_\uparrow$ and $\boldsymbol{\psi}_\downarrow$, respectively. Inspired by the Ising model that the transition temperature is proportional to the exchange interaction [28], we can identify the exchange interaction term between the spin-up and spin-down sublattices to be $(b_0' - b_0''\tau)\Re[\boldsymbol{\psi}_\uparrow^* \cdot \boldsymbol{\psi}_\downarrow]$. Then the Landau expansion in the presence of $\boldsymbol{H}$ is

$$F_H = \frac{1}{2}[F(\eta, \boldsymbol{\psi}_\uparrow)|_{b_0'=b_0''=0} + F(\eta, \boldsymbol{\psi}_\downarrow)|_{b_0'=b_0''=0}] + (b_0' - b_0''\tau)\Re[\boldsymbol{\psi}_\uparrow^* \cdot \boldsymbol{\psi}_\downarrow] - \mu_0 \boldsymbol{M} \cdot \boldsymbol{H}, \quad (8)$$

where $\boldsymbol{M} = g\mu_B \Re[(1+i)(\boldsymbol{\psi}_\uparrow + \boldsymbol{\psi}_\downarrow)]/4$ is the magnetic moment per formula unit. μ_0 is the vacuum permeability, $g \approx 2$ is the Landé factor, and μ_B is the Bohr magneton. F_H correctly returns to F in Eq. (1) when $\boldsymbol{\psi}_\uparrow = -\boldsymbol{\psi}_\downarrow = \boldsymbol{\psi}$ and $\boldsymbol{H} = \boldsymbol{0}$. Then one can proceed normally with Eq. (8) to calculate the magnetic susceptibility $\chi = (\partial M_1/\partial H)_T$, where H is applied along the direction of the larger spin $\boldsymbol{S}_1$, and M_1 is the magnetization component along the same direction.

The calculated susceptibilities are depicted in Fig. 3. The susceptibilities for the collinear and noncollinear magnetic structures both show two kinks, respectively, at the two different Néel temperatures. This can be a signature to detect the possibly separated AFM transitions in rare earth nickelates. Furthermore, the secondary kink associated with the second AFM transition is qualitatively different between the collinear and noncollinear magnetic structures: $\chi(T)$ at the secondary kink is continuous in the collinear

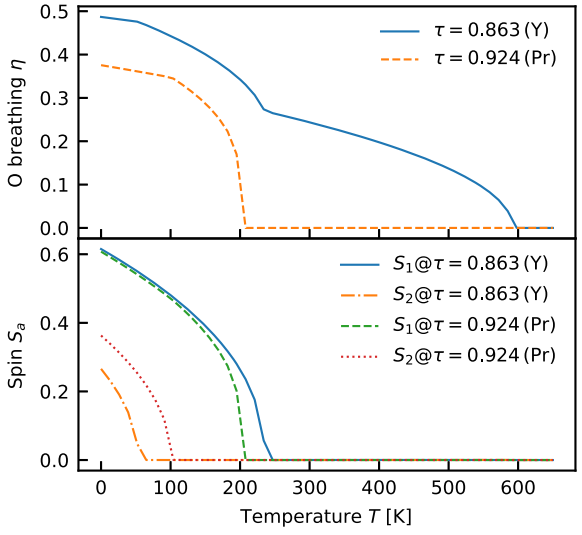

FIG. 2. Calculated O breathing extent (relative change in the O octahedron size, upper panel) and magnitudes of spins on Ni1 and Ni2 sublattices (lower panel) for $R = Y$, Pr.

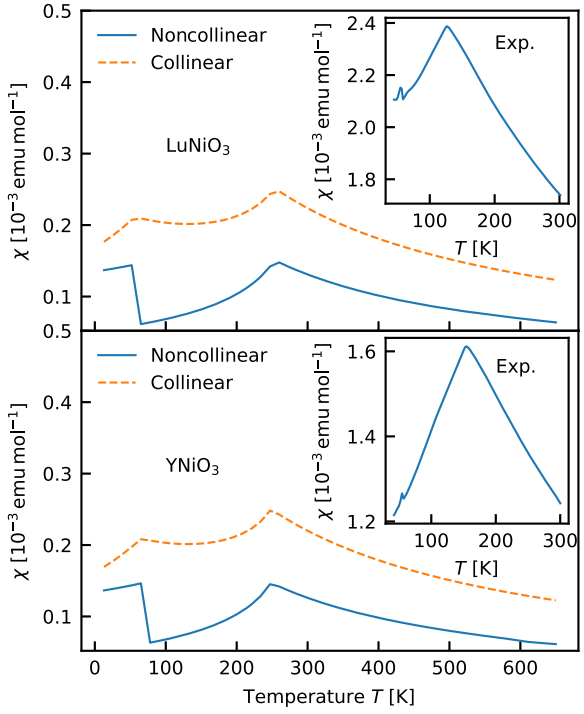

FIG. 3. Calculated magnetic susceptibilities along the direction of the larger spin $\boldsymbol{S}_1$ for $R =$ Lu, Y. For the collinear structure, we set the free parameter $b_1' = 0$, while for the noncollinear structure, we set the free parameter $b_1'' = 0$. The insets are the susceptibilities measured experimentally in the corresponding bulk single crystals [27].

structure, whereas it jumps abruptly in the noncollinear structure. These different degrees of discontinuity result from the different directions of the smaller spin $\boldsymbol{S}_2$ (along $\boldsymbol{H}$ in the collinear structure, while perpendicular to $\boldsymbol{H}$ in the noncollinear structure) at the second AFM transition.

The insets in Fig. 3 show the susceptibilities measured recently in $LuNiO_3$ and $YNiO_3$ bulk single crystals [27]. Although the calculated values of the susceptibilities deviate significantly from the measured ones (which is not surprising due to the simplicity of the Landau model), we see clearly two kinks on each of the measured susceptibilities, confirming our predictions and thus solving the overlooked puzzle on the nature of the secondary kink. The predicted second AFM transition temperatures are also in good agreement with the experiment. While the primary kink is continuous, the secondary kink is clearly discontinuous, which is consistent with our prediction for the noncollinear magnetic structure, thus demonstrating that the magnetic structure of bulk nickelates should be noncollinear.

In conclusion, we investigated by symmetry consideration the AFM transitions in rare earth nickelates focusing on their sublattice-dependent characteristics. For the noncoincident MI and AFM transitions, the AFM transitions on the two nonequivalent Ni sublattices must occur at different Néel temperatures, whereas for the coincident transitions, they can be either separated or concurrent. The Landau parameters fitted to the first-principles ground state energies support the separated AFM transitions for the coincident MI and AFM transitions. These characteristic differences, as well as the formation of nonzero magnetic moments with unequal magnitudes on the two Ni sublattices, are all induced by the monoclinic O breathing mode. The separated AFM transitions lead to two kinks on the temperature-dependent magnetic susceptibility with the secondary kink being continuous in the collinear magnetic structure but discontinuous in the noncollinear structure. We found clear evidence of such a secondary discontinuous kink in an existing magnetic susceptibility measurement for bulk single-crystalline nickelates, thus a strong indication that the magnetic structure of bulk nickelates is noncollinear. We expect our findings to shed new light on the long-standing debate on the magnetic structure of bulk nickelates and to have important implications for other magnetically ordered systems possessing similar symmetry breaking.

This work was supported as part of the Computational Materials Sciences Program funded by the U.S. Department of Energy, Office of Science, Basic Energy Sciences, under Award No. DE-SC0020145.

*yxs187@psu.edu
†lqc3@psu.edu

[1] S. Catalano, M. Gibert, J. Fowlie, J. Íñiguez, J.-M. Triscone, and J. Kreisel, Rare-earth nickelates $RNiO_3$: Thin films and heterostructures, Rep. Prog. Phys. **81**, 046501 (2018).

[2] J. B. Torrance, P. Lacorre, A. I. Nazzal, E. J. Ansaldo, and C. Niedermayer, Systematic study of insulator-metal transitions in perovskites $RNiO_3$ (R = Pr, Nd, Sm, Eu) due to closing of charge-transfer gap, Phys. Rev. B **45**, 8209 (1992).

[3] H. Guo, Z. W. Li, L. Zhao, Z. Hu, C. F. Chang, C. Y. Kuo, W. Schmidt, A. Piovano, T. W. Pi, O. Sobolev, D. I. Khomskii, L. H. Tjeng, and A. C. Komarek, Antiferromagnetic correlations in the metallic strongly correlated transition metal oxide $LaNiO_3$, Nat. Commun. **9**, 43 (2018).

[4] J. A. Alonso, J. L. García-Muñoz, M. T. Fernández-Díaz, M. A. G. Aranda, M. J. Martínez-Lope, and M. T. Casais, Charge Disproportionation in $RNiO_3$ Perovskites: Simultaneous Metal-Insulator and Structural Transition in $YBiO_3$, Phys. Rev. Lett. **82**, 3871 (1999).

[5] U. Staub, G. I. Meijer, F. Fauth, R. Allenspach, J. G. Bednorz, J. Karpinski, S. M. Kazakov, L. Paolasini, and F. d'Acapito, Direct Observation of Charge Order in an Epitaxial $NdNiO_3$ Film, Phys. Rev. Lett. **88**, 126402 (2002).

[6] I. I. Mazin, D. I. Khomskii, R. Lengsdorf, J. A. Alonso, W. G. Marshall, R. M. Ibberson, A. Podlesnyak, M. J. Martínez-Lope, and M. M. Abd-Elmeguid, Charge Ordering as Alternative to Jahn-Teller Distortion, Phys. Rev. Lett. **98**, 176406 (2007).

[7] T. Mizokawa, D. I. Khomskii, and G. A. Sawatzky, Spin and charge ordering in self-doped Mott insulators, Phys. Rev. B **61**, 11263 (2000).

[8] H. Park, A. J. Millis, and C. A. Marianetti, Site-Selective Mott Transition in Rare-Earth-Element Nickelates, Phys. Rev. Lett. **109**, 156402 (2012).

[9] S. Johnston, A. Mukherjee, I. Elfimov, M. Berciu, and G. A. Sawatzky, Charge Disproportionation without Charge Transfer in the Rare-Earth-Element Nickelates as a Possible Mechanism for the Metal-Insulator Transition, Phys. Rev. Lett. **112**, 106404 (2014).

[10] A. Subedi, O. E. Peil, and A. Georges, Low-energy description of the metal-insulator transition in the rare-earth nickelates, Phys. Rev. B **91**, 075128 (2015).

[11] J. L. García-Muñoz, J. Rodríguez-Carvajal, and P. Lacorre, Sudden appearance of an unusual spin density wave at the metal-insulator transition in the perovskites $RNiO_3$ (R = Pr, Nd), Europhys. Lett. **20**, 241 (1992).

[12] M. T. Fernández-Díaz, J. A. Alonso, M. J. Martínez-Lope, M. T. Casais, and J. L. García-Muñoz, Magnetic structure of the $HoNiO_3$ perovskite, Phys. Rev. B **64**, 144417 (2001).

[13] V. Scagnoli, U. Staub, A. M. Mulders, M. Janousch, G. I. Meijer, G. Hammerl, J. M. Tonnerre, and N. Stojic, Role of magnetic and orbital ordering at the metal-insulator transition in $NdNiO_3$, Phys. Rev. B **73**, 100409(R) (2006).

[14] Y. Bodenthin, U. Staub, C. Piamonteze, M. García-Fernández, M. J. Martínez-Lope, and J. A. Alonso, Magnetic and electronic properties of $RNiO3$ (R = Pr, Nd, Eu, Ho and Y) perovskites studied by resonant soft x-ray magnetic powder diffraction, J. Phys. Condens. Matter **23**, 036002 (2011).

[15] A. Frano, E. Schierle, M. W. Haverkort, Y. Lu, M. Wu, S. Blanco-Canosa, U. Nwankwo, A. V. Boris, P. Wochner, G. Cristiani, H. U. Habermeier, G. Logvenov, V. Hinkov, E. Benckiser, E. Weschke, and B. Keimer, Orbital Control of Noncollinear Magnetic Order in Nickel Oxide Heterostructures, Phys. Rev. Lett. **111**, 106804 (2013).

[16] S. B. Lee, R. Chen, and L. Balents, Landau Theory of Charge and Spin Ordering in the Nickelates, Phys. Rev. Lett. **106**, 016405 (2011).

[17] A. Mercy, J. Bieder, J. Íñiguez, and P. Ghosez, Structurally triggered metal-insulator transition in rare-earth nickelates, Nat. Commun. **8**, 1677 (2017).

[18] O. E. Peil, A. Hampel, C. Ederer, and A. Georges, Mechanism and control parameters of the coupled structural and metal-insulator transition in nickelates, Phys. Rev. B **99**, 245127 (2019).

[19] A. B. Georgescu and A. J. Millis, Quantifying the role of the lattice in metal–insulator phase transitions, Commun. Phys. **5**, 135 (2022).

[20] H. T. Stokes, D. M. Hatch, and B. J. Campbell, ISO-IR, ISOTROPY Software Suite, 2022.

[21] H. T. Stokes, B. J. Campbell, and R. Cordes, Tabulation of irreducible representations of the crystallographic space groups and their superspace extensions, Acta Crystallogr. Sect. A **69**, 388 (2013).

[22] J. Rodríguez-Carvajal, S. Rosenkranz, M. Medarde, P. Lacorre, M. T. Fernandez-Díaz, F. Fauth, and V. Trounov, Neutron-diffraction study of the magnetic and orbital ordering in $^{154}SmNiO_3$ and $^{153}EuNiO_3$, Phys. Rev. B **57**, 456 (1998).

[23] J. Pérez-Cacho, J. Blasco, J. García, M. Castro, and J. Stankiewicz, Study of the phase transitions in $SmNiO_3$, J. Phys. Condens. Matter **11**, 405 (1999).

[24] I. Vobornik, L. Perfetti, M. Zacchigna, M. Grioni, G. Margaritondo, J. Mesot, M. Medarde, and P. Lacorre, Electronic-structure evolution through the metal-insulator transition in $RNiO_3$, Phys. Rev. B **60**, R8426 (1999).

[25] J. L. García-Muñoz, J. Rodríguez-Carvajal, and P. Lacorre, Neutron-diffraction study of the magnetic ordering in the insulating regime of the perovskites $RNiO_3$ (R = Pr and Nd), Phys. Rev. B **50**, 978 (1994).

[26] J. Varignon, M. N. Grisolia, J. Íñiguez, A. Barthélémy, and M. Bibes, Complete phase diagram of rare-earth nickelates from first-principles, npj Quantum Mater. **2**, 21 (2017).

[27] Y. M. Klein, M. Kozłowski, A. Linden, P. Lacorre, M. Medarde, and D. J. Gawryluk, $RENiO_3$ single crystals (RE = Nd, Sm, Gd, Dy, Y, Ho, Er, Lu) grown from molten salts under 2000 bar of oxygen gas pressure, Cryst. Growth Des. **21**, 4230 (2021).

[28] J. H. Van Vleck, On the theory of antiferromagnetism, J. Chem. Phys. **9**, 85 (1941).